CeO_2 compatibility with $YBa_2Cu_3O_{7-\delta}$ in superconducting-film multilayers

Yu. A. Boikov,* T. Claeson, and D. Erts†
Department of Physics and Engineering Physics, Chalmers University of Technology and Göteborg University, S-41296 Göteborg, Sweden

F. Bridges and Z. Kvitky
Department of Physics, University of California, Santa Cruz, California 95064
(Received 14 April 1997; revised manuscript received 14 July 1997)

High-quality superconducting ($T_c \approx 90$ K, $j_c > 10^6$ A/cm^2 at 77 K) epitaxial (001) $YBa_2Cu_3O_{7-\delta}$ films were grown by laser ablation on (001) $CeO_2/(1\underline{1}02)$ Al_2O_3. An interaction between $YBa_2Cu_3O_{7-\delta}$ and CeO_2 would influence the structure and the superconducting parameters. A marked degradation of the superconducting transition temperature ($T_c = 74$ K) was observed when twenty 2-nm-thick CeO_2 layers were inserted equidistantly into a (001) $YBa_2Cu_3O_{7-\delta}$ film (200 nm). $BaCeO_3$ crystalline inclusions were detected by x-ray diffraction. X-ray-absorption fine-structure investigations at the Cu-*K* edge indicate that Ce substitutes for Y in $YBa_2Cu_3O_{7-\delta}$. Near-edge x-ray-absorption studies indicate that the valence of Ce incorporated into the $YBa_2Cu_3O_{7-\delta}$ regions of the multilayer structure is also +4. [S0163-1829(97)04541-4]

I. INTRODUCTION

Sapphire is a desired substrate for high-transition temperature (T_c) superconductor structures due to its availability and its low losses at microwave frequencies. Josephson junctions, as with biepitaxial grain boundary devices, may operate at such frequencies and it is therefore desirable to deposit them on sapphire. A problem, however, is the possible diffusion of Al into the high-T_c superconductor, particularly into the junction region, strongly suppressing superconductivity. Thin epitaxial CeO_2 layers have been successfully used as buffers for yttrium[1] and thallium based[2] high-T_c superconducting films on $(1\underline{1}02)$ Al_2O_3 (*R*-cut sapphire). They suppressed a chemical interaction between an $YBa_2Cu_3O_{7-\delta}$ (YBCO) film and Al_2O_3 but traces of Ce that had diffused into YBCO were detected up to a distance of a few *c*-axis lattice parameters from the interface.[3] The interface between an epitaxial, *c* axis oriented (*c* axis normal to the substrate plane) YBCO film and a CeO_2 buffer film was sharp when the superconductor was deposited at a moderately high substrate temperature ($T_s \approx 750$ °C), but a high density of defects was detected in the YBCO film close to the boundary.[4] A pronounced chemical interaction between epitaxially grown CeO_2 buffer and YBCO film layers has been observed[5] if T_s was increased up to 800 °C. $BaCeO_3$ was one of the reaction products.

Thin CeO_2 intermediate epitaxial layers have also been used in different types of biepitaxial heterostructures.[6,7] A biepitaxial 45° crystallographic boundary (in which the *a* axes of YBCO on either side of the boundary are at 45°) should be an effective channel for ion diffusion from YBCO to the substrate and vice versa. It is not yet clear to what extent the parameters of a biepitaxial Josephson barrier may be influenced by stoichiometric deviations in the region of the crystallographic boundary.

In contrast to most rare earths, Ce does not readily substitute into the YBCO lattice. A significant decrease of T_c was observed, however, in bulk YBCO doped with Ce in Ref. 8. The degradation of the superconducting parameters in $Y_{1.2}Ce_xBa_{2.1}Cu_{3.1}O_y$ ($x = 0.1-0.4$; $T_c = 80-54$ K) was attributed to an incorporation of Ce in the YBCO unit cell.[8] The samples were calcined at a temperature of about 900 °C. YBCO grains with orthorhombic and tetragonal structures, as well as inclusions of Y_2BaCuO_5 and $BaCeO_3$ were identified by x-ray diffraction.[8] X-ray diffraction data ($\theta/2\theta$ scans) were also used in Refs. 9 and 10 to study any incorporation of Ce in the YBCO unit cell for bulk alloys. CeO_2 and YBCO were considered to be mutually insoluble in bulk processing.[9,10] While solid-state synthesis typically requires a temperature of 950 °C, the deposition of thin films can take place at a substrate temperature of 650–800 °C. The lower temperature may be a cause of considerably lower diffusivity and hinder phase separation. Fincher and Blanchet[11] obtained a solubility of up to 30% of Ce in laser ablated films of $Y_{1-x}Ce_xBa_2Cu_3O_{7-\delta}$ with only very weak diffraction peaks belonging to undesired $BaCeO_3$ and with a depression in T_c (90–54 K for $x = 0-0.3$), very similar to Pr-doped YBCO.

We will report on results related to the structure and superconductivity of two different heteroepitaxial structures grown on sapphire that involve YBCO films and CeO_2 intermediate layers: (i) 200-nm-thick YBCO films on CeO_2 buffers at different T_s in order to optimize deposition temperature and (ii) a multilayer of 2-nm-thick CeO_2 layers between 10-nm-thick YBCO layers deposited at $T_s = 750$ °C to enhance the inter diffusion between the two constituents. The phase composition is determined by x-ray diffraction while the local structure around the Cu atoms is probed by x-ray-absorption fine structure (XAFS). Superconducting parameters are determined by standard resistance and susceptibility measurements. We will compare with transport measurements on a biepitaxial Josephson junction, that was grown on a CeO_2 buffer layer and a $BaZrO_3$ template and was heat treated at elevated temperature in order to promote additional diffusion along the grain boundary.

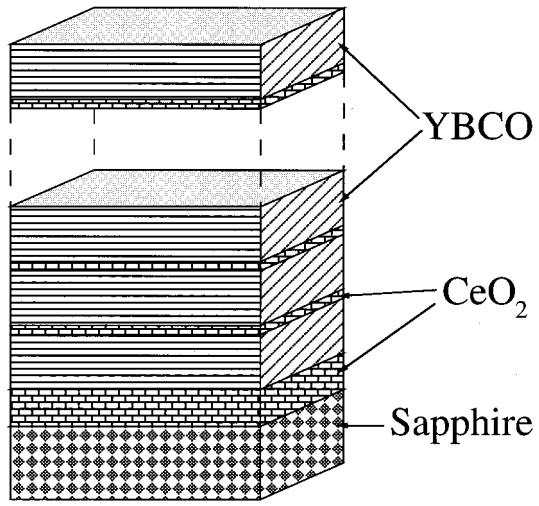

FIG. 1. A multilayer with twenty 2-nm-thick CeO_2 layers inserted equidistantly into an YBCO (200 nm) film grown on (001) $CeO_2 \| (1\bar{1}02)$ Al_2O_3.

II. SAMPLE PREPARATION AND CHARACTERIZATION TECHNIQUE

Laser ablation (KrF, $\lambda = 248$ nm, $\tau = 30$ ns) was used to grow the YBCO and CeO_2 layers grown on $(1\bar{1}02)$ Al_2O_3 buffered by 10 nm (001) CeO_2. The substrate temperature T_s during the growth of the CeO_2 layers was 750 °C. The YBCO films (total thickness of 200 nm) were grown at the surface of the (001) $CeO_2 \| (1\bar{1}02)$ Al_2O_3 at $T_s = 750-790$ °C. Ceramic targets were ablated with an energy density $Q = 2$ J/cm^2 for YBCO and $Q = 1$ J/cm^2 for CeO_2, both in an oxygen atmosphere $p_0 = 0.2$ mbar.

To enhance the inter diffusion at the CeO_2-YBCO interface and study its influence on the structure and superconductivity of YBCO, a multilayer sample consisting of twenty bilayers of 2-nm-thick CeO_2 and 10-nm-thick YBCO layers were deposited to give a total thickness of 240 nm. This forms an YBCO/CeO_2 multilayer, see Fig. 1.

Philips PW 1710 ($\theta/2\theta$) and Siemens D 5000 (ϕ scan) x-ray diffractometers were used for structure and phase analysis of the heterostructures. A thicker CeO_2 film was used in the ϕ scan, (200 nm) YBCO/(50 nm) CeO_2. The surface morphology of the multilayers was studied by atomic force microscopy (AFM).

The superconducting transition temperature T_c for the YBCO in the heterostructures was determined from the temperature dependence of the resistance $R(T)$ and from ''ac'' magnetic susceptibility measurements where the influence of the superconductor on the mutual inductance between two coaxial coils was determined. Critical current density j_c was measured in microbridges (4-μm wide and 50-μm long) formed in the YBCO film by photolithography and Ar ion milling.

III. STRUCTURE AND SUPERCONDUCTIVITY RESULTS

The (001) CeO_2 buffer layer was grown epitaxially on the sapphire substrate as verified by x-ray $\theta/2\theta$ and ϕ scans shown in Figs. 2 and 3. To suppress the formation of (111) CeO_2 grains in the buffer layer[12] [instead of the desired (100) epitaxial film], the CeO_2 target was ablated at a relatively low-energy density $Q \approx 1$ J/cm^2.

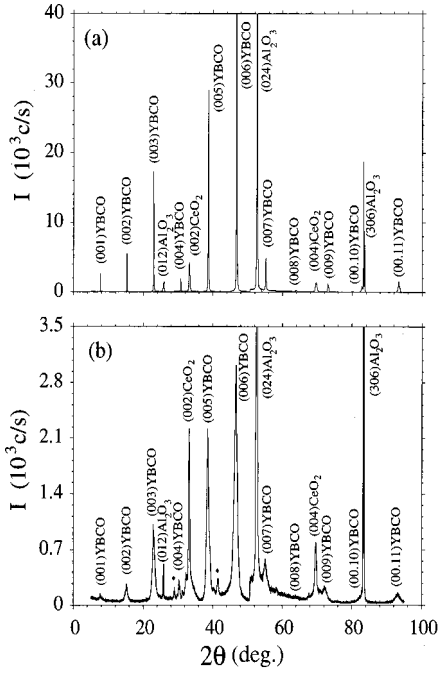

FIG. 2. X-ray diffractograms ($\theta/2\theta$,Cu K_α) for: (a) a (001) YBCO film (200 nm) grown on (001) CeO_2 (10 nm$\|1\bar{1}02$) Al_2O_3 substrate and (b) a YBCO/CeO_2 multilayer on the same substrate; ◆: x-ray peaks for $BaCeO_3$.

High-quality (001) YBCO (200-nm-thick) films were grown epitaxially at the surface of (001) $CeO_2/(1\bar{1}02)$

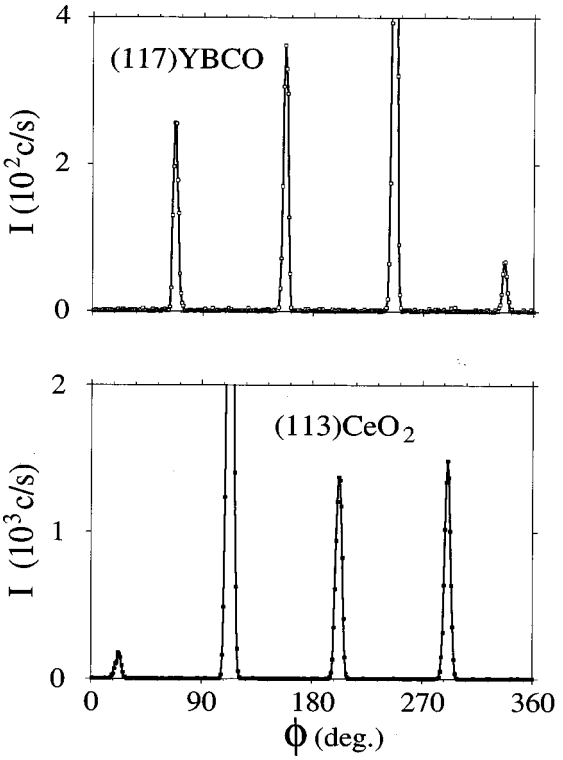

FIG. 3. X-ray ϕ scans (Cu K_α) for (117) YBCO and (113) CeO_2 reflections of a (200 nm) YBCO/(50 nm) CeO_2 epitaxial heterostructure grown on $(1\bar{1}02)$ Al_2O_3.

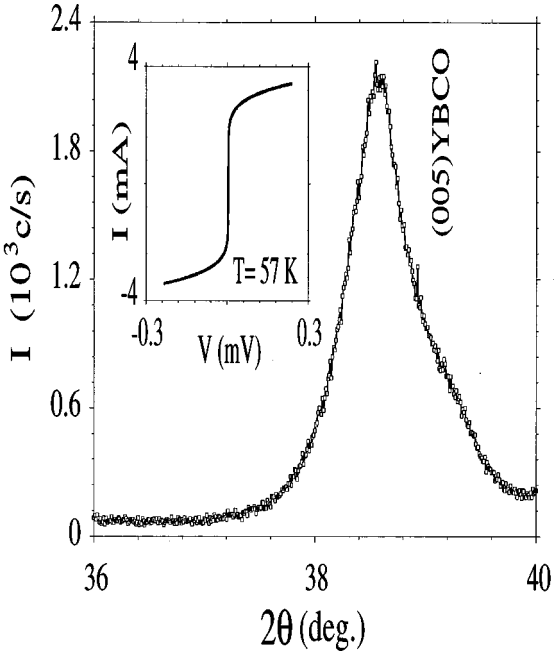

FIG. 4. The (00h) YBCO x-ray peaks were broad and nonsymmetric for the YBCO/CeO_2 multilayers. The (005) YBCO (Cu K_α) peak is shown in the figure. The inset displays an I-V curve for a microbridge etched into a YBCO/CeO_2 multilayer ($T=57$ K). The rounded onset of voltage indicates that it is in a flux flow regime.

Al_2O_3 and the following crystallographic relations were established from the $\theta/2\theta$ and ϕ scans: (001)[010] YBCO$\|$(001)[110] CeO_2. The ab plane of YBCO is rotated 45° relative to CeO_2, see Fig. 3.

The (00n) YBCO and (00h) CeO_2 peaks in the x-ray scans for the YBCO/CeO_2 multilayer were broad and nonsymmetric. A detail of the scan at the YBCO (005) peak is shown in Fig. 4. The lattice parameter for the CeO_2 film ($a=5.393$ Å) was about 0.01 Å smaller than for a bulk ceramic sample. Two additional x-ray peaks were observed in the $\theta/2\theta$ scan for the YBCO CeO_2 multilayer at $2\theta=29.0°$ and 41.5°, see Fig. 2(b).

The surface of the YBCO film, grown on CeO_2 at $T_s=750$ °C was smooth. No spirals were detected in an atomic force microscopy (AFM) study of the YBCO film surface, but a small number of a-axis particles (c axis parallel to the substrate surface) were seen. A high density of pin holes was observed for YBCO films grown at $T_s=785$ °C. This is illustrated in Fig. 5(a). The YBCO/CeO_2 multilayer surface was rough with a high density of outgrowths (of lateral extension $d=0.2-1.5$ μm) as determined by AFM; an image is shown in Fig. 5(b).

Resistive values of T_c, which were determined from the $R(T)$ dependence for YBCO, correlate well with data from ac magnetic susceptibility measurements. This is illustrated in Fig. 6 which shows that the superconducting transition occurs in the range 80–72 K for the YBCO/CeO_2 multilayer (curve 1 for the resistive transition and curve b for the susceptibility). The j_c for the YBCO/CeO_2 multilayer was suppressed in comparison with the value for a single YBCO film on the CeO_2 buffered sapphire; the $j_c(T)$ curve is essentially shifted to lower temperature in accordance with the shift in T_c, see Fig. 6. An example of an I-V curve, from which j_c is determined, is given in the inset of Fig. 4.

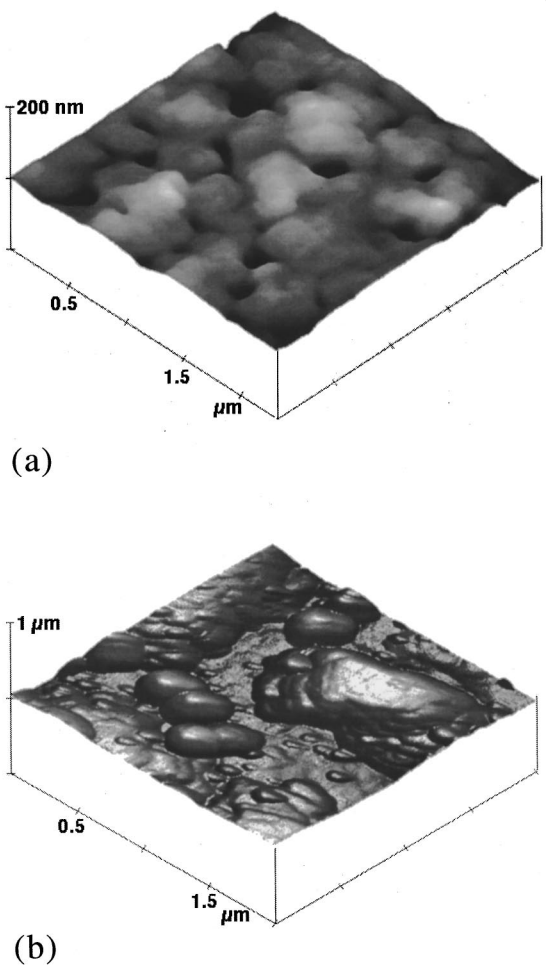

FIG. 5. (a) A high density of pin holes was detected by AFM traces for a (001) YBCO film grown on (001) $CeO_2\|(1\bar{1}02)$ Al_2O_3 at $T_s=785$ °C. (b) A high density of outgrowths was observed by AFM at the surface of a YBCO/CeO_2 multilayer.

The diffusion of Ce and Ba ions should be much larger along a grain boundary at $T\approx700$ °C than for the case of a single c-axis oriented YBCO film on a CeO_2 buffer. To compare the situations, we have investigated the transport properties of biepitaxial Josephson junctions that were formed upon CeO_2 and $BaZrO_3$ ($d=10-80$ nm, $T_s=735$ °C, $Q=2$ J/cm^2, $p_0=0.2$ mbar) layers. [This resulted in a biepitaxial, 45° crystallographic boundary between two YBCO grains upon each type of buffer and template materials. Details of the epitaxial relations for the layers in the (001) YBCO$\|$(110) $BaZrO_3\|$(001) CeO_2 heterostructure and the superconducting film parameters have been discussed separately.[13]] In order to enhance a stoichiometric distortion at the grain boundary, the biepitaxial heterostructures were heat treated in oxygen at 700 °C for 15 min. Current-voltage (I-V) characteristics of the biepitaxial Josephson junctions were tested before and after the treatment. The transition width was broadened 3 to 4 K and the normal state resistance R_n increased about a factor of 2 (from 3.3 to 5.3 Ω) while the critical current I_c decreased about the same amount (from 106 to 61 μA) after the biepitaxial junction had been annealed. The change with a factor of 2 is not very pronounced,

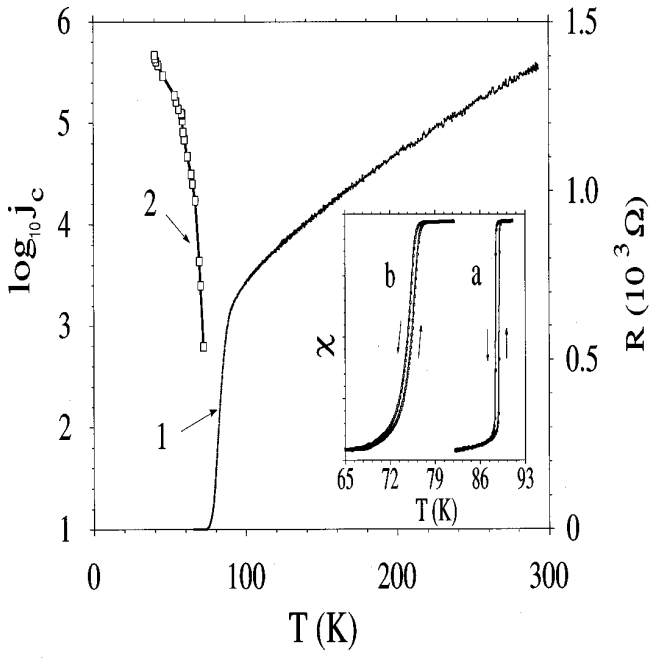

FIG. 6. Temperature dependencies of the resistance (1) and critical current density (2) of a YBCO/CeO_2 multilayer grown on (001) $CeO_2\|(1\underline{1}02)$ Al_2O_3. The inset shows $\chi(T)$ for a YBCO epitaxial film (a) and a YBCO/CeO_2 multilayer (b) grown on buffered sapphire as above.

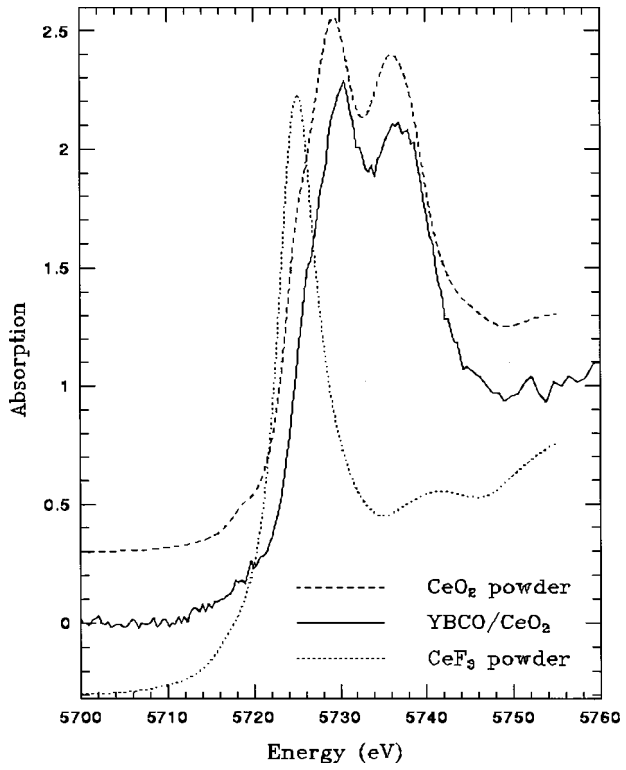

FIG. 7. Ce-L_{III} x-ray-absorption edges for a YBCO/CeO_2 multilayer and two powder standards having a Ce valence of $+3$ (CeF_3) and $+4$ (CeO_2).

taking into account any exponential dependence on thickness in a grain boundary junction (assuming it is characterized as an insulating barrier). Roughly the same behavior has been observed for biepitaxial junctions on a $SrTiO_3$ substrate with a CeO_2 buffer, which speaks against a diffusion of Al from the sapphire being the cause of the change. The characteristic voltage, I_cR_n, for the biepitaxial junctions did not change during the treatment. It remained roughly the same, 325–350 μV (at 36 K). These results indicate that any possible diffusion of Ce along the grain boundary did not affect its properties appreciably.

In contrast to the case of biepitaxial junctions, there were no indications of either dc or ac Josephson effects in I-V characteristics for microbridges prepared from the multilayer. A flux flow regime was observed in the I-V curve if the current through the multilayer bridge exceeded the critical value, see the inset in Fig. 4.

IV. X-RAY-ABSORPTION FINE STRUCTURE

X-ray-absorption fine structure (XAFS) experiments are well suited to study the local environment around absorbing atoms. The method uses monochromatic photons that are swept in energy around and, in particular, above the absorption edge of one of the atoms in the compound of interest. Electrons, that are excited from inner core K or L shells of the atom by the absorbed photons, will be backscattered by neighboring atoms and interfere with the outgoing electron wave, producing fine structure (oscillations) in the x-ray absorption at energies above the edge energy. The fine structure in the absorption vs photon energy can inform on the number of scattering neighbors at different distances, the kind of neighbors (by specific phase shifts in the XAFS functions), and the spread in distances (i.e., disorder expressed as a Debye-Waller-type broadening). Shifts in the energy of the absorption edge, or in the shape of the edge, provides information on the valence state of the absorbing atom.

Fluorescence x-ray-absorption data were collected for the Cu-K and Ce-L_{III} edges on the multilayer sample and for the Cu-K edge for pure YBCO thin film samples. Full XAFS scans were obtained for the Cu-K edge, but only near edge structure data for the Ce-L_{III} edge. (The Ba and Ce edges are so close in energy that their XAFS interfere strongly, which prevents a meaningful analysis.) A Si (220) crystal monochromator on beam line 4-3 at the Stanford Synchrotron Radiation Laboratory (SSRL) and a 13 element Ge detector array were used to collect the fluorescent x-ray photons from the sample. The film was placed at a ''magic'' angle of 55° relative to the incident radiation (the angle was chosen to minimize any preferential scattering due to the strong polarization of the synchrotron radiation and the film orientation) and cooled to about 50 K in a He flow cryostat. The energy resolution of the experiment was estimated to be 3 eV.

Figure 7 shows the Ce-L_{III} absorption edges of the multilayer sample as well as of two standards of different valence—CeO_2 (of valence Ce^{4+}) and CeF_3 (valence Ce^{3+}). The two standard samples were in powder form, with thicknesses of the order of an absorption length, and the data were taken in the transmission mode. (A CeF_4 standard, which is not shown here, gave the same double hump structure as CeO_2 did.) Both the shape and the energy of the absorption edge for the multilayer sample resemble those of the 4^+ standard. There is no clear evidence of a shoulder on the leading edge that would be an indication of a mixture of formally 3^+ and 4^+ valences. Simulations, that used combi-

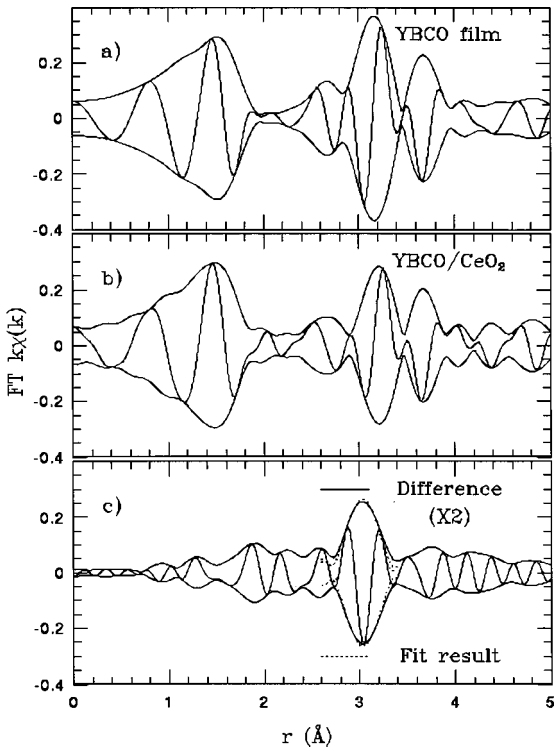

FIG. 8. Fourier transforms of the Cu K-edge XAFS $k\chi(k)$ for (a) a reference YBCO film, (b) the YBCO/CeO_2 multilayer, and (c) the difference between (a) and (b). The fast oscillation is the real (Re) part of the transform while the envelope is $\pm(\mathrm{Re}^2+\mathrm{Im}^2)^{1/2}$. The only dramatic changes occur around 3.0 Å, i.e., in the region of Cu-Y and Cu-Ba bonds in YBCO. The transforms here and in Fig. 9 were taken from 3.5 to 14 $\mathrm{Å}^{-1}$, with a 0.3 $\mathrm{Å}^{-1}$ Gaussian window. The dotted curves in (c) depict fits over the range 2.8–3.25 Å. The sample temperature was 50 K.

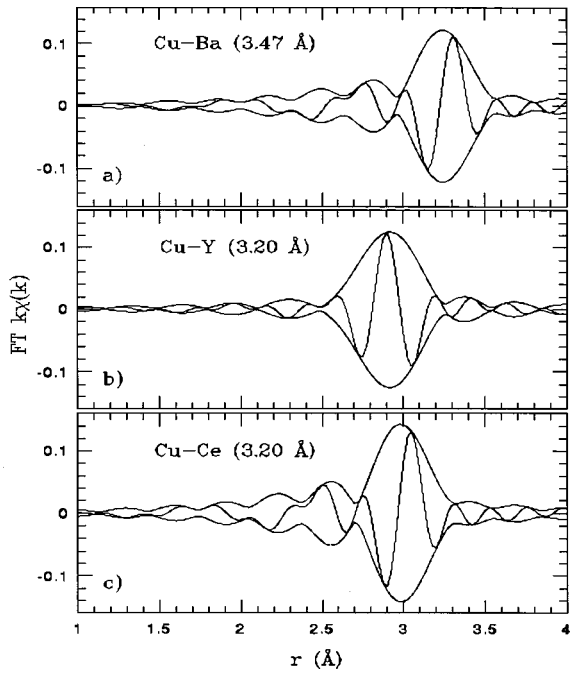

FIG. 9. Fourier transforms of $k\chi(k)$ for Cu K-edge functions generated theoretically by the FEFF6 code (Ref. 15) for Cu-Ba, Cu-Y, and Cu-Ce atom pairs at distances corresponding to YBCO. Note the difference in the phase of the real part of the transform between back scattering from Y and Ce; this gives rise to destructive interference. The FT range is the same as in Fig. 8.

nations of the 3^+ and 4^+ edge standards, showed that the presence of 10% of Ce in its 3^+ state should be discernible. Note that there appears to be a small shift in energy of the double peak spectra for the multilayer compared to the powder CeO_2 sample. We had no reference sample (to check for energy shifts) for the thin film samples as there was no x-ray transmission through the thick substrate. Estimates from other traces suggest that drifts of the monochromator may be of the order of up to 1 eV. This is about the size of the observed shift.

The energy data of the Cu-K XAFS were converted to k space (with the photoelectron wave vector $k=[(2m_e/h^2)(E-E_0)]^{1/2}$, where E_0 is the K-edge threshold energy) and Fourier transformed (FT) to r space using a procedure described earlier.[14] The FT yields peaks in r space corresponding to different radial distances to neighbors of the excited atoms; the peak positions are slightly shifted in distance ($\sim$0.2–0.4 Å) from the atom-pair spacing due to phase shifts at the scattering and absorbing atoms and must be compared to standard XAFS functions in order to obtain the atom-pair distances.

The FT of the Cu-K XAFS of the multilayer is compared with the corresponding data for a reference YBCO film (100 nm on a MgO substrate), taken during the same run, as shown in Fig. 8. As expected (for the ''magic'' angle), the YBCO film gave essentially the same FT as a powder sample. Note that the main difference between the two film FT's occurs around 3 Å (including phase shifts), with a depressed peak for the multilayer. This is clearly seen in Fig. 8(c) which displays the difference between the two. This difference function has a large amplitude at 3.0 Å, near the position where the Cu-Y peak (3.2 Å) has a maximum and the Cu-Ba peaks (3.37 and 3.47 Å) are close to a minimum (See Fig. 9). In addition, the difference plot has a *minimum* at 3.4 Å where the sum of the two Cu-Ba peaks would have a maximum. Thus it appears that the Cu-Ba peak is relatively unchanged. No difference was discernible in the first peak, which is very sensitive to any changes in the positions of the nearest-neighbor O atoms.

In order to extract numerical information on how much of the Ce that might be incorporated at different lattice sites, fits of the r space Cu-K XAFS for the multilayer were done using standards of Cu-Y, Cu-Ba, and Cu-Ce obtained from the FEFF6 code.[15] Such fits have proven to be very successful.[16]

V. DISCUSSION

During the initial stage of YBCO ablation, there are Y, Ba, and Cu ions, neutral atoms, and different types of oxides in the plasma plume from the target and in the adsorbed phase of YBCO at the substrate surface. The Ba in the nucleating YBCO reacts with the CeO_2 buffer at substrate temperatures $>700\,^{\circ}\mathrm{C}$. The main products of the chemical interaction between the nucleated YBCO and the CeO_2 are Y_2BaCuO_5, $BaCeO_3$, and CuO according to Ref. 5. The intensity of the reaction depends crucially on the processing temperature. At $T_s<750\,^{\circ}\mathrm{C}$, the contamination of the reac-

tion products at the CeO_2 surface during the initial stage of the YBCO film formation is low and it does not interfere drastically with the YBCO film nucleation. (001) YBCO is well matched to (001) CeO_2 and *c*-axis oriented YBCO nuclei become stable due to the low values of the surface free energy for (001) planes. This low surface energy is the driving force for *c*-axis YBCO nucleation, as discussed in Ref. 17. The Ce and Ba ion inter diffusion along the *c* axis in YBCO epitaxial films is slow at $T_s < 750\,^{\circ}\mathrm{C}$, as shown in Ref. 3. Therefore, a thin layer (a few YBCO unit cells) at the YBCO-CeO_2 interface acts as a buffer and inhibits Ce diffusion into the rest of the superconducting film.

For the YBCO films on CeO_2, $T_c = 88-90\,\mathrm{K}$ and $j_c > 10^6\ \mathrm{A/cm^2}$ (at 77 K) agree well with the data reported in Refs. 3 and 6. The sharp drop in the ac magnetic susceptibility signal at $T = T_c$ is an indication of the phase purity, i.e., an absence of macroscopic size inclusions of a low-T_c phase in the YBCO film volume.

The observed decrease of the *c* axis of the epitaxial YBCO film, down to 11.66 Å, see e.g., Fig. 2(a) is an indication of a high level of tensile strains in the ab-plane due to differences in the thermal expansion coefficients of YBCO and Al_2O_3.

The high density of pin holes which was detected by AFM on YBCO films, that had been deposited at relatively high temperature on CeO_2 ($T_s > 780\,^{\circ}\mathrm{C}$), is an indication of an increased chemical interaction between YBCO and the CeO_2 buffer. Second phase inclusions at the surface of the substrate or in the growing film may cause pin-hole nucleation. At high T_s, the YBCO-CeO_2 interaction results in the formation of inclusions of a second phase ($BaCeO_3$) at the CeO_2 surface. The density of YBCO nuclei formed at the surface of $BaCeO_3$ is depressed because of a large mismatch in lattice parameters between YBCO and $BaCeO_3$ (cubic, $a = 4.397$ Å, Ref. 18). This restricts the growth of an YBCO layer over the $BaCeO_3$ inclusions or over other second phase precipitates incorporated in the superconducting film volume.

YBCO and CeO_2 interaction in multilayers The influence of the interaction between YBCO and CeO_2 on the structure and properties of the superconducting film became much more pronounced when the effective area of the YBCO-CeO_2 interfaces increased, as in the case of the YBCO/CeO_2 multilayer. The x-ray data, Fig. 2(b), for a YBCO/CeO_2 multilayer is a clear indication of a chemical reaction between YBCO and CeO_2 at $T_s = 750\,^{\circ}\mathrm{C}$. The observed x-ray peaks at $2\theta = 29.0°$ and 41.5° may be identified as (110) and (200) reflections of $BaCeO_3$ having an effective lattice parameter of 4.35 Å. The parameter is smaller, about 0.04–0.05 Å, as compared with bulk data,[18] possibly due to doping of the $BaCeO_3$ inclusions by Y from YBCO. Due to the preferential orientation of the YBCO film, and possibly the $BaCeO_3$ precipitates, it was not possible to make any sensible estimate of the amount of $BaCeO_3$ that was included. The observed high density of outgrowths at the surface of the YBCO/CeO_2 multilayer may be the result of a segregation of CuO, $YBaCuO_5$, and possibly, $Y_2Cu_2O_5$ inclusions.[19] For example CuO particles typically float to the surface of the film as a YBCO layer is formed beneath.[20]

We can compare with another system, $(Y,Pr)Ba_2Cu_3O_{7-\delta}$, where Pr also gives a depression of T_c. The T_c's of YBCO/$(Pr,Y)Ba_2Cu_3O_{7-\delta}$ based multilayers[21] are about 83 K even if the superconducting layers in the superlattices are as thin as four stacked YBCO unit cells. The j_c's at 4.2 K are very close to values typically observed for epitaxial thick YBCO films on $SrTiO_3$ substrates. In our case, the T_c decrease of YBCO in the multilayer was about 16 K as determined from resistive measurements. The long low-temperature tail observed for the transition in the susceptibility vs temperature curve is an indication of a further depression of T_c in a fraction of the YBCO film volume. A deterioration of the YBCO stoichiometry due to interaction with CeO_2 may be one of the reasons for the T_c and j_c suppressions, particularly an incorporation of Ce in the YBCO unit cell.

We saw a large change in the FT of the Cu-edge XAFS just where the Cu-Y peak is. In Fig. 9(c) we show that the real part of the FT of a Cu-Ce peak at 3.2 Å is nearly 180° out of phase with that for the Cu-Y peak. Consequently, any substitution of Ce on the Y site will have a double effect on the Cu-Y peak amplitude. In contrast, the Cu-Ba transform [Fig. 9(a)] shows a minimum at the distance where this difference is the largest.

We therefore interpret the difference spectrum shown in Fig. 8(c) as arising from a partial replacement of Y by Ce in the YBCO lattice. To test this hypothesis, we fit the peak region (2.8–3.3 Å) to a sum of two theoretical standards (FEFF6 code, Ref. 15) with equal (but opposite) amplitudes; a Cu-Y standard and a (negative) Cu-Ce standard. The amplitudes were kept equal in magnitude and the Cu-Y position fixed (within 0.02 Å) in this fit. (In other fits we also held the two Debye-Waller factors equal to reduce the number of fit parameters.) Good fits were obtained for about 25–35 % of the Y replaced by Ce (the best fit actually gave 29%). If we let the Cu-Y and Cu-Ce distances vary, the Cu-Y peak is at 3.22 Å and the Cu-Ce peak at 3.24 Å; 0.02, and 0.04 Å longer, respectively, than for Cu-Y in YBCO. The small increase of the Cu-Ce distance is not unexpected since Ce has a larger radius (in either valence state). An example of one of these fits is given by the dotted curves of Fig. 8(c).

We also considered the possibility of Ce substituting into the Ba site and carried out fits of the difference data to a sum of Cu-Ba and Cu-Ce standards, with Cu-Ba constrained to be close to the Cu-Ba distances in pure YBCO. These attempts gave poor fits with goodness-of-fit parameters roughly two orders of magnitude worse. Hence, we conclude that little of the Ce went into the Ba site.

The maximum possible number of Cu-Ce distances at the YBCO/CeO_2 interfaces is insufficient to explain the large concentration of Ce replacing Y. In our multilayer, we have nine unit cells of YBCO and then a layer of CeO_2 on each side; the number of Cu-Y pair distances per Cu atom is $\frac{8}{3}$ in the unit cell (normalizing for the three Cu layers in the unit cell). If we assume that the interface occurs with a Ce layer adjacent to a Cu-O plane, then there are $\frac{4}{3}$ Cu-Ce pairs per Cu atom at the interface. Thus with nine units cells and two interfaces there are $\frac{72}{3}$ Cu-Y/Ce pair distances in total, with $\frac{64}{3}$ within the YBCO layer and $\frac{8}{3}$ pair distances at the interfaces. The ratio would be $\frac{8}{64} = \frac{1}{8}$ or 12%. To explain part of the Cu-Ce signal in terms of the interfaces we must also assume that the interface bonds have essentially the same

length (although the Ce-Ce distance in CeO_2 is significantly longer at 3.83 Å) and are not badly distorted. Furthermore, it is not clear that YBCO nucleates with a CuO_2 layer closest to the CeO_2 film. One might rather expect a Ba-O layer to be the matching one. The best fit[4] of experimental transmission electron microscope images to image simulations for YBCO/CeO_2 interfaces was obtained when the BaO layer was chosen to be the first one on top of the CeO_2 layer. (If the interface bonds are more disordered and/or shifted in position, the Cu-Ce contribution from these bonds would be broadened, the suppression of the Cu-Y peak from the interface bond contribution would not be so large and the Cu-Ce should be modeled as two peaks at different distances. Fitting the Cu-Ce distribution with one peak works well; the peak has a narrow width and a slight shift of only 0.02 Å from the Cu-Y peak position in this film.)

Thus, it appears that a significant fraction of the Ce is going into the YBCO but it is difficult to estimate more precisely the fraction. It looks like at least 15–20 % of the Y in the YBCO has been replaced by Ce, and possibly 30 % if interfacial Cu-Ce distances are not important. Comparing with the data[11] for suppression of T_c due to Ce substitution in thin films of YBCO, we would expect a solubility of 15–20 % for a T_c of about 70–75 K. In our case, there might be a complicating gradient in the Ce concentration in the YBCO layer, but the estimated concentrations seem to be consistent.

The shape and position of the Ce-L_{III} absorption edge indicate that Ce is primarily in the 4^+ valence state of CeO_2; 10% of the 3^+ state should have been detected. Since a large portion of the Ce has diffused into the YBCO, this suggests that the Ce valence is also $+4$ in YBCO. It may explain why Ce substitution strongly suppresses T_c as Ce would remove a hole from the (hole conducting) Cu-O plane and localize it. However, the assumption is not without complications. Ce and Pr give the largest depression of superconductivity of rare earth substitutions, they are both large (being the lightest of the rare earths) and $4f$ electrons may extend far enough to hybridize with O $2p$ electrons. However, different experiments on the Pr compound give different valences, in particular, spectroscopic methods would give $+3$ for Pr. X-ray-absorption near-edge structure indicated[22,23] that Pr is trivalent in PBCO while the effective valence increased for small concentrations of Pr in YBCO (Lytle *et al.*[24] give $3.25+$ for 20% Pr in YBCO.) A theory that combines different valences is due to Fehrenbacher and Rice.[25] Two electronic configurations are favored: a $Pr^{3+}(4f^2)$-O state and an admixture of $Pr^{4+}(4f^1)$-O and $Pr^{3+}(4f^2\underline{L})$-O states, where $\underline{L}$ indicates that the hole does not reside within the electron structure of Pr but, rather, is within the ligand. The most energetically favorable configuration is the state $+3$ but with the other two configurations present about 30–40 % of the time, causing pair breaking. XAFS measurements[26] on Pr-doped YBCO indicated a broadening of the Pr-O nearest-neighbor distances (with some Pr-O distances shorter by about 0.2 Å). This would be consistent with a mixture of Pr^{3+} and the hybridized state involving a ligand hole and to a formal valence slightly above $+3$ for the Pr ion in YBCO. In our case, the near-edge absorption indicates mainly a $4+$ state for Ce in YBCO.

VI. CONCLUSIONS

High-quality (001) YBCO epitaxial films were grown on R-cut sapphire buffered by 10 nm (001) CeO_2. Second phase inclusions, which involve $BaCeO_3$ and other by-products of a YBCO-CeO_2 reaction, provoked a pin-hole formation in the superconducting film grown on CeO_2/Al_2O_3 at $T_s > 780\,^{\circ}\mathrm{C}$. A pronounced chemical interaction between YBCO (200 nm) and CeO_2 was detected by x-ray diffraction and XAFS experiments when twenty 2-nm-thick CeO_2 layers were inserted equidistantly into the superconducting film. Extra diffraction lines showed the occurrence of $BaCeO_3$ and pronounced changes of the Cu K-edge XAFS, in the second neighbor region corresponding to Y, indicate that Ce substitutes for Y. The near-edge results for the Ce L_{III} edge showed that the Ce incorporated into YBCO is primarily in the $+4$ valence state. Both the change in stoichiometry and the substitution with Ce affected superconductivity negatively.

ACKNOWLEDGMENTS

Help from and discussions with C. Booth are gratefully acknowledged. The research was initiated within the framework of scientific cooperation on high-T_c superconductivity between the Swedish and Russian Academies of Sciences. Financial support for the study was also received by the EU INTAS program (Project No. 94-3861), the Russian Foundation on Basic Research (Project No. 95-02-04186-a), the U.S. National Science Grant No. DMR-92-05204, and the Swedish Materials Consortia. Part of the experiments were performed at the Stanford Synchrotron Radiation Laboratory, which is operated by the U.S. Department of Energy, Division of Chemical Sciences, and by the NIH, Biomedical Resource Technology Program, Division of Research Resources. The XAFS work (F.B.) was supported in part by NSF Grant No. DMR-92-05204.

*Also at Ioffe Physico-Technical Institute RAS, 194021 St. Petersburg, Russia.

†Also at Institute of Chemical Physics, Latvia University, Riga, Latvia.

[1] X. D. Wu, R. C. Dye, R. E. Muenchausen, S. R. Foltyn, M. Maley, A. D. Rollet, A. R. Garcia, and N. S. Nogar, Appl. Phys. Lett. **58**, 2165 (1991).

[2] W. L. Holstein, L. A. Parisi, D. W. Face, X. D. Wu, S. R. Foltyn, and R. E. Muenchausen, Appl. Phys. Lett. **61**, 982 (1992).

[3] M. W. Denhott and J. D. McCaffrey, J. Appl. Phys. **70**, 3986 (1991).

[4] A. L. Vasiliev, G. Van Tendeloo, A. Amelinchx, Yu. A. Boikov, E. Olsson, and Z. G. Ivanov, Physica C **244**, 373 (1995).

[5] G. I. Skofrounick, A. H. Carim, S. R. Foltyn, and R. E. Muenchausen, J. Mater. Res. **8**, 2785 (1993).

[6] L. P. Lee, K. Char, M. S. Colclough, and G. Zaharchuk, Appl. Phys. Lett. **59**, 3051 (1991).

[7] Yu. A. Boikov, Z. G. Ivanov, A. L. Vasiliev, and T. Claeson, J. Appl. Phys. **77**, 1654 (1995).

[8] C. J. Kim, K. B. Kim, S. C. Kwon, I. S. Chang, and D. E. Won, J. Mater. Sci. Lett. **11**, 346 (1992).

[9] E. V. Sampathkumatan, A. Susuki, K. Kohn, T. Shibuys, A. To-

hdake, and M. Ishikama, Jpn. J. Appl. Phys., Part 2 , **27**, L584 (1988).
[10] P. Sladeczek, U. Neukirch, C. T. Simmons, D. Strebed, C. Lauschat, D. D. Sarma, and G. Kaindl, Physica C **153–155**, 916 (1988).
[11] C. R. Fincer, Jr. and G. B. Blanchet, Phys. Rev. Lett. **67**, 2902 (1991).
[12] Yu. A. Boikov and T. Claeson, Supercond. Sci. Technol. (to be published).
[13] Yu. A. Boikov, Z. G. Ivanov, and T. Claeson, Phys. Solid State (to be published).
[14] T. M. Hayes and J. B. Boyce, in *Solid State Physics*, edited by H. Ehrenreich, F. Seitz, and D. Turnbull (Academic, New York, 1982), Vol. 37, p. 173; F. Bridges, C. H. Booth, and G. G. Li, Physica B **208&209**, 121 (1995).
[15] S. I. Zabinsky, A. Ankudinov, J. J. Rehr, and R. C. Albers, Phys. Rev. B **52**, 2995 (1995).
[16] G. G. Li, F. Bridges, and C. H. Booth, Phys. Rev. B **52**, 6332 (1995).
[17] Yu. A. Boikov, Z. G. Ivanov, E. Olsson, V. A. Danilov, T. Claeson, M. Sheglov, and D. Erts, Phys. Solid State **37**, 478 (1995).
[18] R. W. G. Wyckoff, *Crystal Structure*, 2nd ed. (Interscience, New York, 1964), Vol. 2, p. 241.
[19] Yu. A. Boikov, Z. G. Ivanov, E. Olsson, J. A. Alarco, G. Brorsson, and T. Claeson, J. Appl. Phys. **72**, 199 (1992).
[20] P. Lu, J. Zhao, C. S. Chern, Y. Q. Li, G. A. Kulesha, B. Gallois, D. Norris, B. Keat, and F. Cosandey, J. Mater. Res. **7**, 1993 (1992).
[21] C. Kwon, X. X. Xi, S. Bhattacharya, C. Doughty, T. Venkatesan, H. Zhang, J. W. Lynn, J. L. Peng, and Z. Y. Li, Appl. Phys. Lett. **62**, 1289 (1993).
[22] E. E. Alp, G. K. Shenoy, L. Soderholm, G. L. Goodman, D. G. Hinks, and B. W. Veal, in *High-Temperature Superconductors*, edited by M. B. Brodsky, R. C. Dynes, K. Kitazawa, and H. L. Tuller, MRS Symposia Proceedings No. 99 (Materials Research Society, Pittsburgh, 1988), p. 177.
[23] S. Horn, J. Cai, S. A. Shaheen, Y. Jeon, M. Croft, C. L. Chang, and M. L. denBoer, Phys. Rev. B **36**, 3895 (1987).
[24] F. W. Lytle, G. van der Laan, R. B. Greegor, E. M. Larson, C. E. Violet, and J. Wong, Phys. Rev. B **41**, 8955 (1990).
[25] R. Fehrenbacher and T. M. Rice, Phys. Rev. Lett. **70**, 3471 (1993).
[26] C. H. Booth, F. Bridges, J. B. Boyce, T. Claeson, Z. X. Zhao, and P. Cervantes, Phys. Rev. B **B49**, 3432 (1994).